Human Molecular Genetics, 2010, Vol. 19, No. 19 **3721–3733**
doi:10.1093/hmg/ddq286
Advance Access published on July 16, 2010

Mitochondrial GLUT10 facilitates dehydroascorbic acid import and protects cells against oxidative stress: mechanistic insight into arterial tortuosity syndrome

Yi-Ching Lee[1,2], Hsun-Yi Huang[1], Chia-Jung Chang[1], Chao-Hung Cheng[1] and Yuan-Tsong Chen[1,3,*]

[1]Institute of Biomedical Sciences, Academia Sinica, Taipei 11529, Taiwan, Republic of China, [2]Graduate Institute of Integrated Medicine, China Medical University, Taichung 404, Taiwan, Republic of China and [3]Department of Pediatrics, Duke University Medical Center, Durham, NC 27710, USA

Received June 7, 2010; Revised June 25, 2010; Accepted July 5, 2010

Mutations in glucose transporter 10 (GLUT10) alter angiogenesis and cause arterial tortuosity syndrome (ATS); however, the mechanisms by which these mutations cause disease remain unclear. It has been reported that in most cells, mitochondria are the major source of reactive oxygen species (ROS). Moreover, mitochondria are known to incorporate as well as recycle vitamin C, which plays a critical role in redox homeostasis, although the molecular mechanism(s) underlying mitochondrial vitamin C uptake are poorly understood. We report here that GLUT10 localizes predominantly to the mitochondria of smooth muscle cells and insulin-stimulated adipocytes, where GLUT10 is highly expressed. We further demonstrate that GLUT10 facilitates transport of L-dehydroascorbic acid (DHA), the oxidized form of vitamin C, into mitochondria, and also increases cellular uptake of DHA, which in turn protects cells against oxidative stress. This protection is compromised when GLUT10 expression in mitochondria is inhibited. In addition, we found that aortic smooth muscle cells from GLUT10-mutant mice have higher ROS levels than those from wild-type mice. Our results identify the physiological role of GLUT10 as the mitochondrial DHA transporter, and demonstrate that GLUT10 protects cells from oxidative injury. Furthermore, our findings provide a mechanism to explain the ascorbate in mitochondria and show how loss-of-function GLUT10 mutations may lead to arterial abnormalities in ATS. These results also reinforce the importance of vitamin C and ROS in degenerative diseases.

INTRODUCTION

The solute carriers 2A (SLC2A) family of glucose and polyol facilitative transporters comprises 13 members (1). Based on sequence homology, the glucose transporter (GLUT) family has been grouped into three subclasses: classes I, II and III (2). Despite their sequence similarity, these GLUTs have different specificities for transporting various hexose substrates (2). The tissue- and cell-specific expression levels of different GLUT isoforms have been well characterized, providing further evidence for the specific physiological roles of the various GLUT isoforms in hexose transport and the control of whole-body glucose homeostasis. However, the transport functions and physiological roles of the most recently discovered GLUT6-12 isoforms in the metabolism of hexose, and perhaps other substrates, remain to be determined.

Glucose transporter 10 (GLUT10), encoded by the *SLC2A10* gene, belongs to the class III GLUT family. The human *SLC2A10* gene is located on chromosome 20q12–13.1, a region that has been shown to be associated with type 2 diabetes (3,4). However, evidence for an association

*To whom correspondence should be addressed at: Institute of Biomedical Sciences, Academia Sinica, 128 Academia Road, Section 2, Nankang, Taipei 11529, Taiwan, Republic of China. Tel: +886 227899104; Fax: +886 227825573; Email: chen0010@ibms.sinica.edu.tw

between mutations or polymorphisms in GLUT10 and type 2 diabetes is inconclusive (5–8). Recent studies have revealed that the connective tissue disorder arterial tortuosity syndrome (ATS) is caused by loss-of-function mutations in the human *SLC2A10* gene (9). ATS is an autosomal recessive disorder characteristic by tortuosity, elongation, stenosis, and aneurysm formation in the major arteries secondary to disorganization of elastic fibers in the medial layer of the arterial wall. ATS patients usually also present with connective tissue manifestations, such as soft, hyperextensible skin, joint laxity, contractures and soft nasal cartilage. The loss of GLUT10 function has been proposed to lead to a decrease in intracellular glucose level and activation of the transforming growth factor β (TGFβ) pathway through decorin, which is transcriptionally upregulated by glucose (9). However, glucose tolerance tests have shown that glucose and insulin profiles are normal in patients and carriers with pathogenic mutations in *SLC2A10* (10). It is therefore unlikely that GLUT10 function is needed to maintain a proper glucose gradient across the plasma membrane. Although it has been shown that GLUT10 mediates D-glucose uptake in *Xenopus* oocytes (11), the physiological transport function of GLUT10 in mammalian cells has not yet been demonstrated.

To understand the physiological function of GLUT10 and the molecular mechanisms by which GLUT10 deficiency leads to ATS, we examined the subcellular localization, transport function and roles of GLUT10 in physiologically relevant cells. We found that GLUT10 is mainly localized to the mitochondria of aortic smooth muscle cells and insulin-stimulated adipocytes. GLUT10 was highly expressed in both cell types and mediated transport of L-dehydroascorbic acid (DHA), the oxidized form of vitamin C, into mitochondria. GLUT10-mediated DHA transport into mitochondria augmented vitamin C accumulation in both mitochondria and cells, and protected cells from oxidative damage by reducing the production of reactive oxygen species (ROS). An examination of ROS levels in aortic smooth muscle cells cultured from GLUT10-mutant mice and their wild-type littermates showed that under oxidative stress conditions, ROS levels were higher in the smooth muscle cells of mutant mice carrying functionally deficient GLUT10. These results define the physiological function of GLUT10 and provide a mechanism to account for ascorbate in mitochondria. Furthermore, these results explain how loss-of-function mutations of GLUT10 may lead to ATS.

RESULTS

Tissue distribution and aortic expression pattern of GLUT10 in the mouse

To determine the physiological function of GLUT10, we first determined the tissue distribution of GLUT10 mRNA transcripts in mouse by real-time reverse transcriptase–polymerase chain reaction (RT–PCR). GLUT10 mRNA is highly expressed in the stomach, white adipose tissue, pancreas and aorta (Supplementary Material, Fig. S1A). Based on the published results from a GCRMA-processed GeneAtlas U133A array (SymAtlas, Genomics Institute of the Novartis Research Foundation), GLUT10 mRNA is also highly expressed in human aortic smooth muscle cells and adipocytes. Because the most significant clinical presentations of GLUT10 loss-of-function mutations in human and mouse involve the aorta (9,12), we further analyzed the cell-type-specific expression of GLUT10 mRNA in aortic tissue by *in situ* hybridization. The results showed that GLUT10 mRNA is highly expressed in the smooth muscle cell layers of mouse aortic tissues, a distribution that was verified by staining for the smooth muscle cell marker desmin (Supplementary Material, Fig. S1B).

Subcellular localization of GLUT10 in adipocytes and smooth muscle cells

Where a protein is localized within a cell often provides important insight into its function. Thus, as a first step toward defining the function of GLUT10, we sought to determine its subcellular localization. To this end, we generated two constructs, GLUT10/EGFP and GLUT10/Myc-His, to express EGFP (enhanced green fluorescent protein) and Myc-His fusion proteins of GLUT10, respectively (Fig. 1A). We then examined the intracellular distribution of the fusion proteins in transiently transfected mouse fibroblast NIH3T3 cells. Both GLUT10/EGFP and GLUT10/Myc-His fusion proteins showed a similar perinuclear localization in NIH3T3 cells (Fig. 1B), a pattern that contrasted sharply with the even distribution of EGFP observed in control cells expressing an EGFP-only vector (Fig. 1B). The GLUT10/EGFP construct was used for subsequent subcellular compartment co-localization studies. Using different subcellular compartment trackers to provide a more refined assessment of intracellular distribution in NIH3T3 cells, we found that GLUT10/EGFP was localized to the Golgi apparatus (Fig. 1C). To determine GLUT10 subcellular localization in physiological relevant cells, we then determined GLUT10/EGFP subcellular localization in adipocytes using fully differentiated 3T3-L1 cells, which have an adipocyte-like phenotype and are sensitive to insulin. The differentiated 3T3-L1 adipocytes were stained with Oil-Red-O to demonstrate the presence of triglyceride droplets (Fig. 2A). In these differentiated 3T3-L1 adipocytes, GLUT10 was localized to the Golgi apparatus in 3T3-L1 cell lines stably expressing the GLUT10/EGFP fusion protein (Fig. 2B). Proteins in the Golgi apparatus are modified and packaged into vesicles for distribution to different cell compartments, as appropriate for the function of each protein. Because GLUT4 is known to redistribute from an intracellular compartment to the plasma membrane in response to insulin and play an important role in insulin-induced glucose uptake in adipocytes (13), we examined whether insulin treatment induced a similar redistribution of GLUT10. Interestingly, a portion of GLUT10/EGFP was localized to mitochondria after insulin treatment (Fig. 2B). These results were further confirmed by immunoblotting analysis, which showed that GLUT10/EGFP was present at high levels in the mitochondria-enriched fraction after insulin stimulation (Supplementary Material, Fig. S2). No GLUT10/EGFP surface expression was detected following insulin treatment (Fig. 2B). Thus, GLUT10 primarily localizes to the Golgi apparatus in adipocytes under basal conditions and translocates to mitochondria upon insulin stimulation.

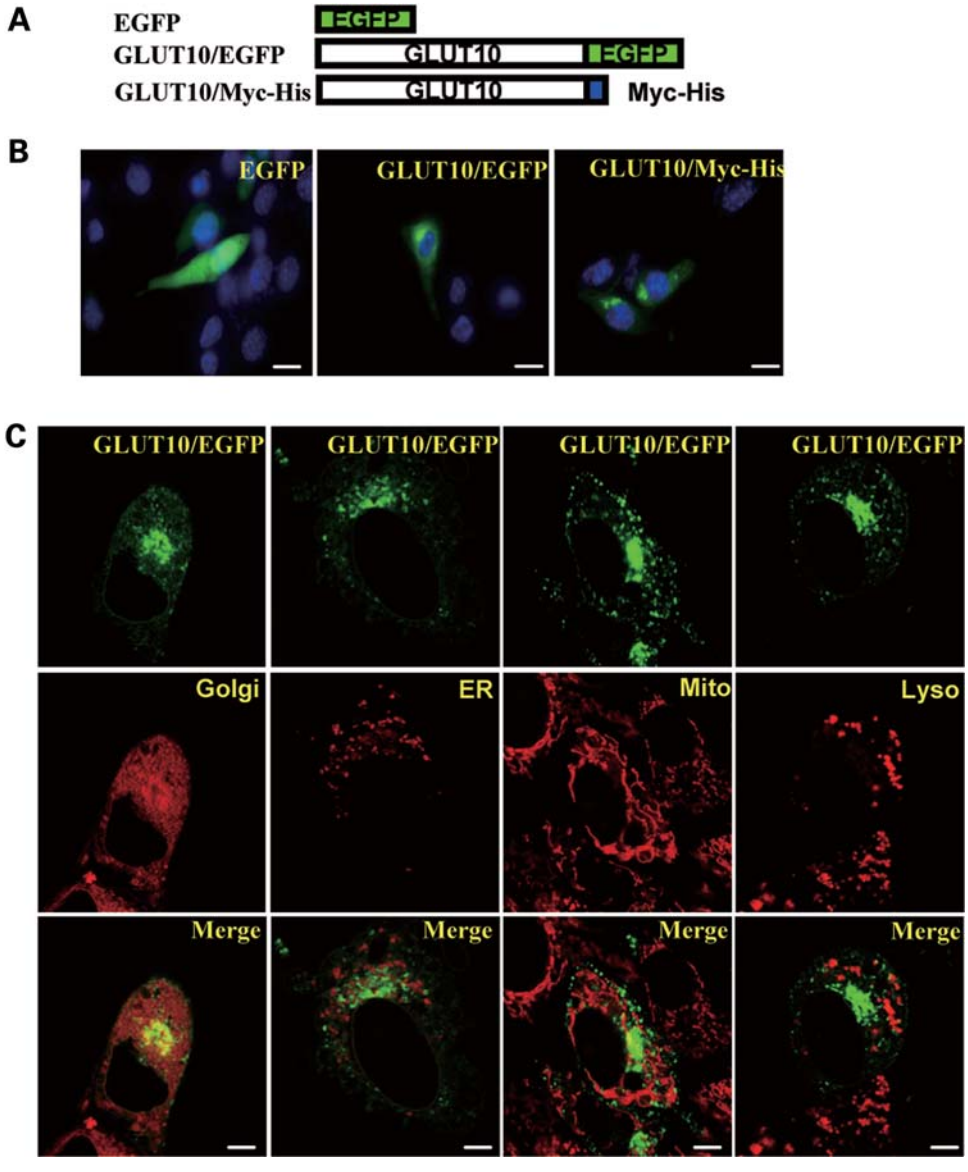

Figure 1. GLUT10 subcellular localization in NIH3T3 cells. (**A**) A schematic of EGFP, and C-terminally tagged GLUT10/EGFP and GLUT10/Myc-His fusion proteins. (**B**) Fluorescence detection of EGFP and GLUT10/EGFP in live NIH3T3 cells transiently expressing the indicated protein. Immunofluorescence detection of GLUT10/Myc-His in fixed NIH3T3 cells transiently expressing the GLUT10/Myc-His protein. The cell images were collected by inverted fluorescence microscopy at a magnification of ×400. Scale bars, 50 μm. (**C**) The co-localization of GLUT10/EGFP with different subcellular compartment trackers. Green, EGFP signals representing GLUT10/EGFP localization; red, subcellular compartment tracker signals for Golgi (Golgi), endoplasmic reticulum (ER), mitochondria (Mito) and lysosome (Lyso); yellow, merged signal representing co-localization. Note that GLUT10/EGFP co-localized with the Golgi tracker. Scale bars, 10 μm.

We further examined the subcellular localization of GLUT10 in aortic smooth muscle cells using the A10 rat aortic smooth muscle cell line. Unexpectedly, ∼50% of GLUT10/EGFP was localized to the mitochondria in A10 cells under both basal and insulin-stimulated conditions (Fig. 3A). This distribution pattern was confirmed by immunoblotting, which showed that GLUT10/EGFP was prominent in a mitochondria-enriched fraction; in contrast, EGFP was mainly detected in the remaining fraction in control A10 cells expressing EGFP only (Fig. 3B). Taken together, these results indicate that GLUT10 mainly localizes to mitochondria in aortic smooth muscle cells.

Mitochondrial GLUT10 enhances DHA transport into mitochondria and augments ascorbic acid accumulation in cells

We next sought to determine the transport function of mitochondrial GLUT10. Glucose in the cytosolic milieu exists almost entirely as glucose 6-phosphate, which is a non-transportable form of glucose (14); moreover, mitochondria lack the glycolysis pathway, instead using pyruvate as a substrate for the tricarboxylic acid cycle. These observations indicate that mitochondrial GLUT10 may serve a function other than glucose transport. Interestingly, transport of DHA, the

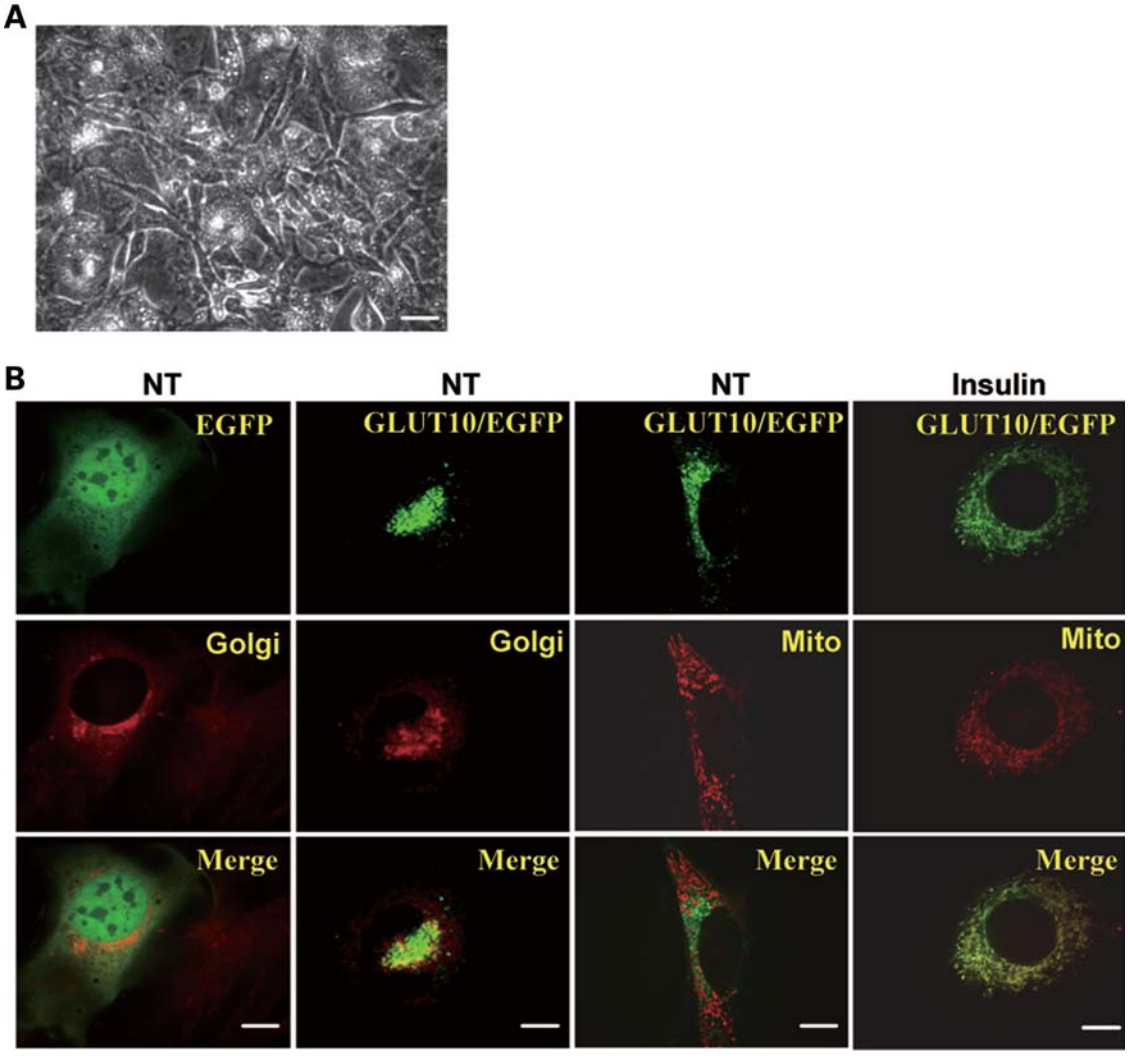

Figure 2. Insulin-stimulated mitochondrial translocation of GLUT10 in differentiated 3T3-L1 cells stably expressed GLUT10/EGFP. (**A**) Differentiated 3T3-L1 adipocytes were stained with Oil-Red-O to demonstrate the presence of triglyceride droplets. The bright-field image was taken under inverted microscopy at a magnification of ×200. Scale bars, 40 μm. (**B**) The GLUT10/EGFP subcellular localization pattern in 3T3-L1 cells was assessed by co-localization with different subcellular compartment trackers. GLUT10/EGFP localized to the Golgi under basal conditions and translocated to mitochondria following insulin stimulation. Green, EGFP signals representing GLUT10/EGFP localization; red, subcellular compartment tracker signals; yellow, merged signal representing co-localization. Golgi, Golgi tracker; Mito, Mitotracker; NT, cells cultured in basal median; Insulin, cells stimulated with insulin. Scale bars, 10 μm.

oxidized form of ascorbic acid, by GLUT1, GLUT 3 and GLUT 4 has been reported (15–17), and it is well documented that mammalian mitochondria accumulate and recycle vitamin C (ascorbic acid) (18). However, the mechanisms underlying mitochondrial ascorbic acid uptake have remained unclear. Mammalian mitochondria cannot transport ascorbic acid (18,19). Therefore, we reasoned that mitochondrial GLUT10 might function as a facilitative DHA transporter and play a role in mitochondrial ascorbic acid accumulation. To test this hypothesis, we sought to determine whether exogenously expressed mitochondrial GLUT10 enhanced entry of intracellular DHA into mitochondria. We first examined the ability of differentiated 3T3-L1 and A10 cells to take up DHA. We observed a dose-dependent increase in intracellular ^{14}C in response to extracellularly applied ^{14}C-labeled DHA in both cell types (Supplementary Material, Fig. S3A and B). We next measured the amount of ^{14}C entering the mitochondria in A10 cells expressing EGFP or GLUT10/EGFP. Incubating cells with ^{14}C-labeled DHA led to a concentration-dependent increase in ^{14}C in the mitochondria (Fig. 4A). The amount and percentage of ^{14}C entering the mitochondria were increased by exogenous expression of GLUT10/EGFP (Fig. 4A). Interestingly, although cell surface GLUT10/EGFP was not detected in cells exogenously expressing GLUT10/EGFP, DHA entry into these cells was increased upon exposure to DHA (Fig. 4A). A dose-dependent increase in DHA uptake in response to exogenous expression of GLUT10/EGFP was observed (Fig. 4B), indicating that increased DHA entry into mitochondria might also enhance DHA uptake into cells in the presence of DHA.

To further confirm a role for mitochondrial GLUT10 in enhancing DHA entry into mitochondria, we directly assessed DHA transport into mitochondria using purified mitochondria. DHA was transported in a concentration- and time-dependent

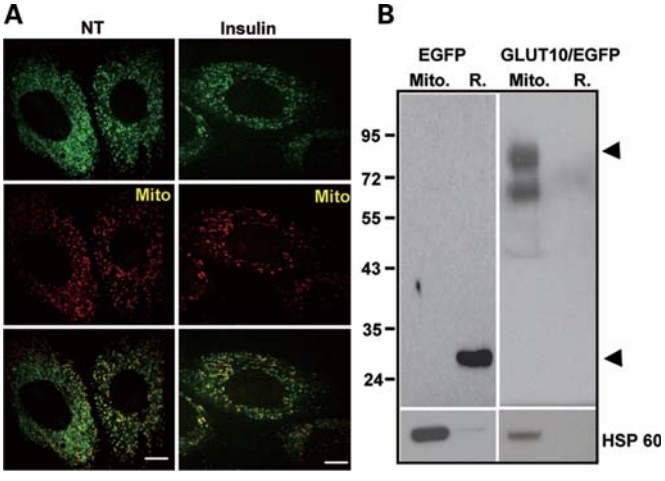

Figure 3. GLUT10 localizes to mitochondria in A10 cells. (**A**) Approximately 50% of GLUT10/EGFP localized to mitochondria under basal (NT) and insulin-stimulated conditions (Insulin). Subcellular localization of transiently expressed GLUT10/EGFP in A10 cells was determined by co-localization with mitochondrial compartment trackers. Green, EGFP signals representing GLUT10/EGFP localization; red, mitochondrial compartment tracker signals (Mito); yellow, merged signal representing co-localization. Scale bars, 10 μm. (**B**) The GLUT10/EGFP fusion protein was primarily detected in a mitochondria-enriched fraction, whereas EGFP was mainly detected in the remainder fraction. Proteins purified from mitochondria (Mito) and a remainder fraction (R) of A10 cells transiently expressing EGFP or GLUT10/EGFP were analyzed for EGFP and mitochondrial proteins by western blotting. GFP, antibodies against GFP; HSP 60, antibodies against heat shock protein 60, a mitochondrial chaperon protein.

manner into mitochondria purified from A10 cells (Fig. 3C and D), saturating after 30 min of incubation (Fig. 3D). DHA-uptake ability was significantly increased in mitochondria purified from GLUT10/EGFP-expressing A10 cells compared with those from EGFP-expressing A10 cells (Fig. 4C and E). Moreover, preincubating purified mitochondria with increasing concentrations of cold D-glucose reduced mitochondrial DHA uptake (Fig. 4E). These results provide additional support for the idea that DHA enters the mitochondria through the glucose transporter GLUT10.

Although these data indicate a DHA-transport function for GLUT10, they do not exclude the possibility that GLUT10 also functions as a mitochondrial glucose transporter under physiological condition. To test this possibility, we incubated A10 cells with ^{14}C-labeled D-glucose and measured ^{14}C accumulation in the cytosol and mitochondria. Most ^{14}C remained in the cytosol (99.97415%), whereas only 0.0258% of ^{14}C entering cells was detected in the mitochondria (Supplementary Material, Fig. S4). These results indicate that D-glucose entered cells and was quickly converted into the non-transportable glucose 6-phosphate, indicating that the physiological role of mitochondrial GLUT10 is DHA transport rather than glucose transport.

To extend these findings to adipocytes, we tested the ability of GLUT10 to transport DHA into the mitochondria in 3T3-L1 cells. Treatment of these cells with insulin, which promotes GLUT10 translocation to mitochondria, induced an increase in ^{14}C entry into mitochondria (Fig. 4F). Exogenous expression of GLUT10/EGFP in insulin-stimulated 3T3-L1 cells further increased ^{14}C mitochondrial entry (Fig. 4F), indicating that insulin-induced translocation of GLUT10 to the mitochondria increases DHA entry into mitochondria. Taken together, these results provide compelling evidence that GLTU10 in mitochondria functions as a DHA transporter.

GLUT10-mediated transport of DHA into mitochondria protects cells from oxidative stress by reducing ROS production

During aerobic respiration, oxidative events in mitochondria are the major source of ROS, which can damage mitochondria and may contribute to the decline in mitochondrial function associated with degenerative diseases. To determine whether mitochondrial GLUT10-mediated transport of DHA into mitochondria plays a physiological role in modulating oxidative stress, we examined ROS production in A10 cells, with or without exogenous GLUT10 expression, under various conditions; total ascorbic acid levels in mitochondria were also determined by high-performance liquid chromatography (HPLC) analysis. Treatment of cells with the oxidative stressor H_2O_2 induced a significant increase in ROS levels in A10 cells (Fig. 5A, compare the control + H_2O_2 group and controls in the overlay histogram and the quantitative data in the right panel). H_2O_2-induced increases in ROS levels were reduced by preloading cells with DHA (Fig. 5A, compare control + DHA + H_2O_2 and control + H_2O_2 treatment groups). ROS levels were further reduced in A10 cells expressing GLUT10/EGFP and preloaded with DHA (Fig. 5A, compare GLUT10 + DHA + H_2O_2 and control + DHA + H_2O_2 treatment groups), an effect that was abolished by inhibiting DHA entry into cells by preincubation with D-glucose (Fig. 5A, compare GLUT10 + D-glu + DHA + H_2O_2 and GLUT10 + DHA + H_2O_2 treatment groups). HPLC analyses showed that mitochondrial ascorbic acid levels in A10 cells were significantly increased under DHA incubation and oxidative stress conditions, and were further increased by exogenously expressed GLUT10 (Fig. 5D). To provide additional evidence that GLUT10-mediated DHA entry into mitochondria reduces cellular ROS production, we reduced endogenous GLUT 10 expression in A10 cells by RNA interference (RNAi), which knocked down GLUT10 mRNA expression by ~80% (Fig. 5E). GLUT10 knockdown in A10 cells abolished the ability of DHA treatment to reduce ROS production under oxidative stress conditions (Fig. 5B, compare control + DHA + H_2O_2 and RNAi + DHA + H_2O_2 treatment groups). We then extended the analysis of ROS production to adipocytes. Preincubation of GLUT10-expressing 3T3-L1 cells with DHA reduced the ROS level under oxidative stress conditions (Fig. 5C, compare GLUT10 + DHA + H_2O_2 and control + H_2O_2 treatment conditions). Importantly, treatment of these cells with insulin, which, as noted above, promotes mitochondrial translocation of GLUT10, induced a significant reduction in intracellular ROS levels (Fig. 5C, compare GLUT10 + insulin + DHA + H_2O_2 and GLUT10 + DHA + H_2O_2 treatment groups). Collectively, these results indicate that mitochondrial GLUT10 facilitates DHA entry into mitochondria and protects cells from oxidative stress by reducing ROS production.

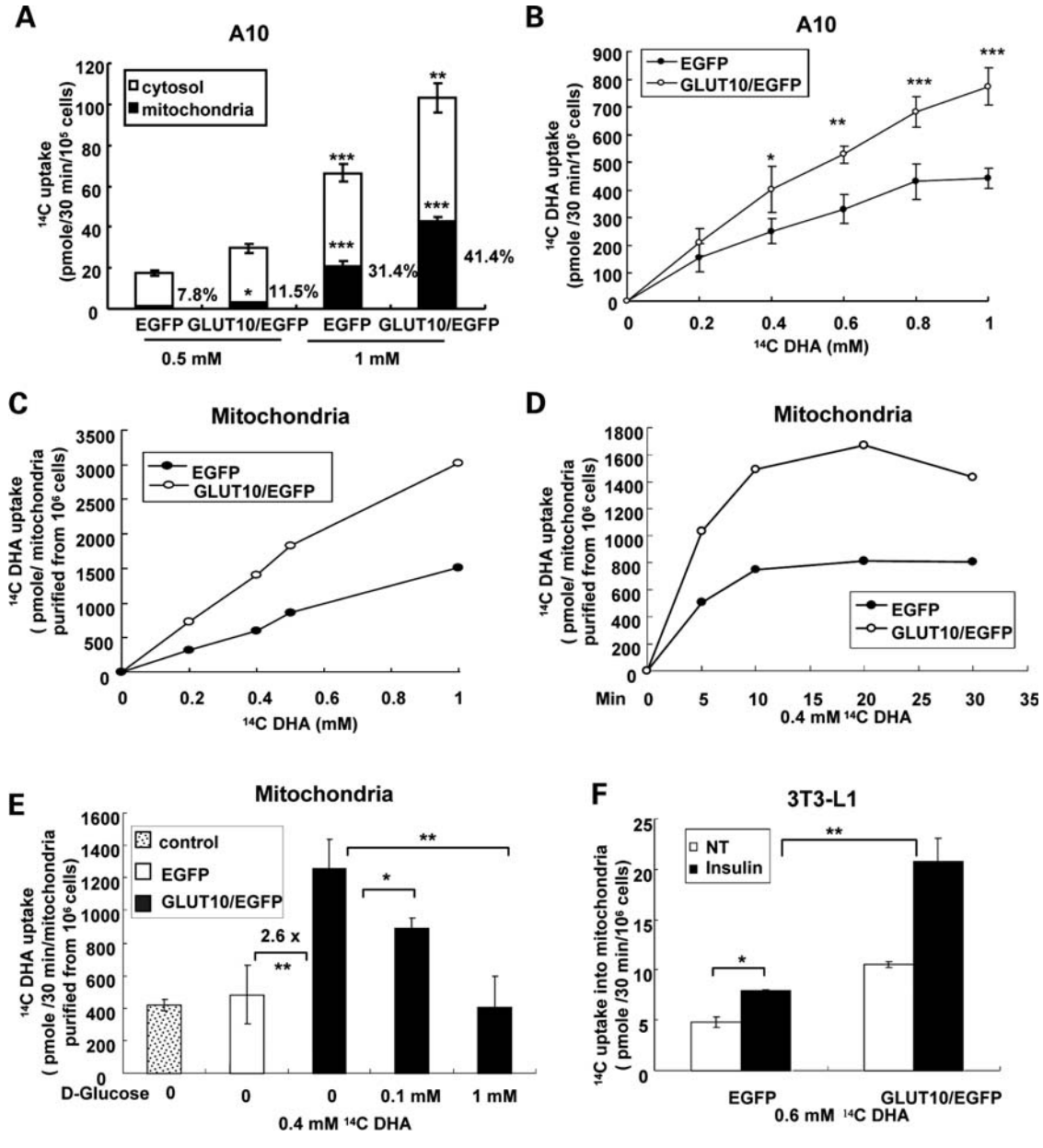

Figure 4. Mitochondrial GLUT10 facilitates DHA transport. (**A**) ^{14}C accumulation in cytosol (open box) and mitochondria (filled box) was determined in A10 cells by incubating A10 cells expressing EGFP or GLUT10/EGFP with 0.5 or 1 mM ^{14}C-labeled DHA. DHA entry into A10 cells and mitochondria was dependent on the extracellular DHA concentration. ^{14}C entry into mitochondria was enhanced by ~2-fold in A10 cells expressing GLUT10/EGFP, and ^{14}C levels in mitochondria were increased by 10% by incubation in 1 mM DHA. (**B**) Intracellular accumulation of ^{14}C in A10 cells expressing EGFP (closed circle) or GLUT10/EGFP (open circle) was determined in cells incubated with the indicated concentration of ^{14}C-labeled DHA. DHA entry into A10 cells was increased in the GLUT10/EGFP-expressed A10 cells in a dose-dependent manner. (**C**) Mitochondria purified from EGFP (closed circle) or GLUT10/EGFP (open circle)-expressed A10 cells were incubated with the indicated concentration of ^{14}C-labeled DHA for 30 min. (**D**) Mitochondria purified from EGFP (closed circle)- or GLUT10/EGFP-expressed A10 cells were incubated with 0.4 mM ^{14}C-labeled DHA for the indicated times. DHA uptake in mitochondria is concentration- and time-dependent and is greater in mitochondria purified from GLUT10/EGFP-expressed A10 cells than in those purified from A10 cells expressing only EGFP (control). (**E**) Mitochondrial DHA-uptake ability was determined in purified mitochondria by incubating with ^{14}C-labeled DHA. DHA-uptake ability was significantly increased in mitochondria purified from A10 cells expressing GLUT10/EGFP compared with A10 cells expressing EGFP only, and DHA-uptake ability in mitochondria was inhibited by preincubating with increasing concentrations of D-glucose. (**F**) DHA entry into mitochondria was determined in 3T3-L1 cells expressing EGFP or GLUT10/EGFP incubated with 0.6 mM ^{14}C-labeled DHA and stimulated with 10 μg/ml insulin (filled box, insulin) or not treated (open box, NT). DHA in mitochondria increased with insulin treatment and was further increased in cells expressing GLUT10/EGFP.

ROS levels are higher in aortic smooth muscle cells of ATS mice than in those of wild-type littermates

Finally, to examine the potential protective role of mitochondrial GLUT10 against oxidative stress in the setting of ATS, we evaluated ROS levels in the aortic smooth muscle cells in ATS mice. This *Glut10*$^{G128E/G128E}$ mouse model, generated in our laboratory, is homozygous for a missense mutation in GLUT10 (G128E) and shows mild phenotypes of abnormal elastogenesis with early elastic fiber proliferation at the age

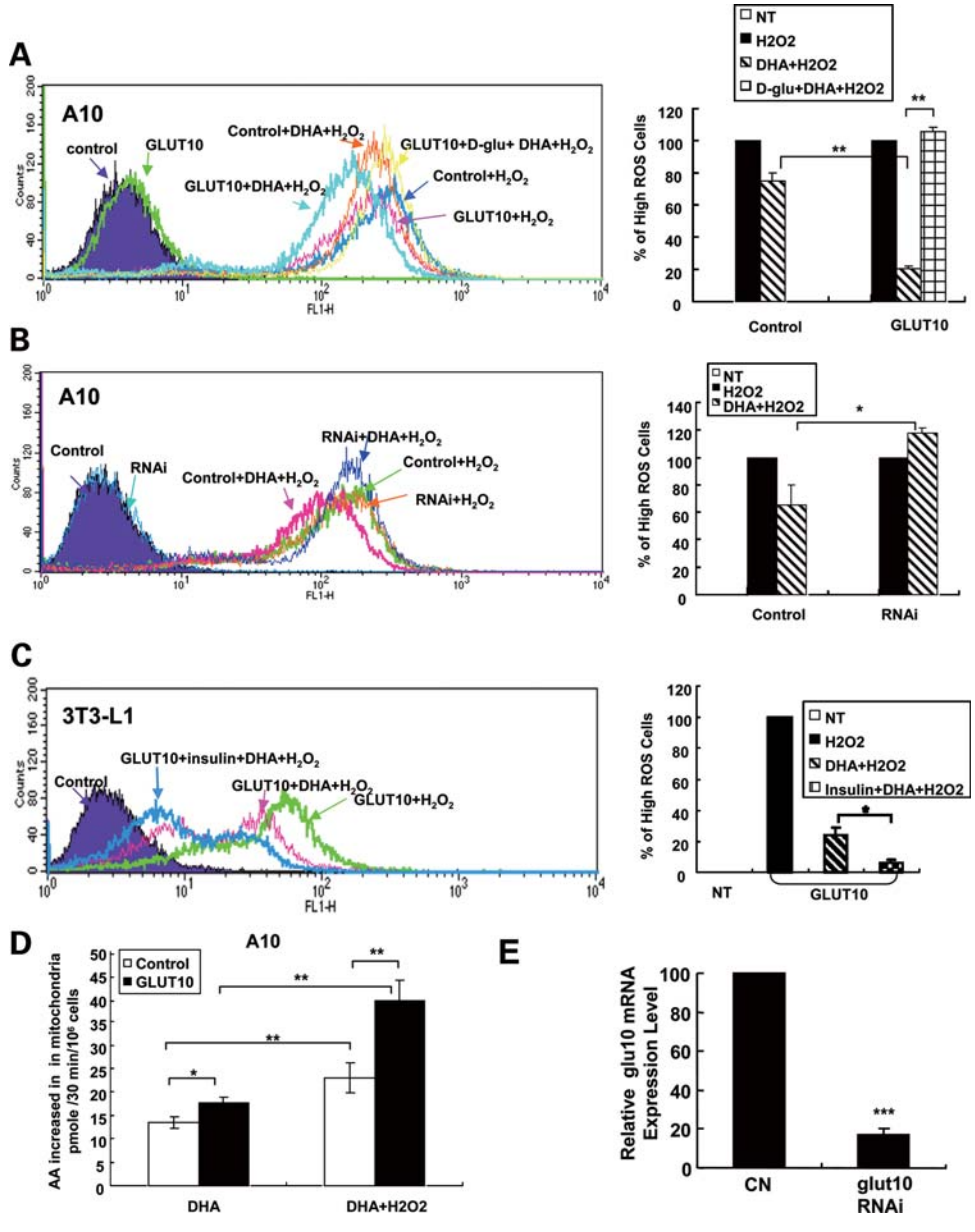

Figure 5. Mitochondrial GLUT10 protects cells from oxidative damage under oxidative stress conditions in the presence of DHA. (**A**–**C**) Intracellular ROS production in cells under various treatment paradigms was detected by H_2DCFDA-staining and analyzed by flow cytometry. The results of overlay histograms from one representative experiment out of three independent experiments are presented. The quantitative data from three independent experiments are shown on the right. The individual treatments are as follows: Control, cells transfected with empty vector; GLUT10, cells expressing GLUT10/Myc-His; H_2O_2, A10 cells treated with 0.5 mM H_2O_2 or 3T3-L1 cells treated with 1 mM H_2O_2; DHA, cells incubated with 1 mM DHA before H_2O_2 treatment; D-glu, cells preincubated with 1 mM D-glucose before incubation with DHA; RNAi, cells transfected with glut10RNAi; Insulin, 3T3-L1 cells treated with 10 μg/ml insulin. (A) A comparison of GLUT10 + DHA + H_2O and control + DHA + H_2O_2 treatment histograms shows that ROS production was decreased in A10 cells expressing GLUT10. This reduction in ROS production was abolished by preincubating cells with D-glucose (compare GLUT10 + D-glu + DHA + H_2O_2 and GLUT10 + DHA + H_2O_2 treatment histograms), which inhibited DHA entry into A10 cells. (B) A comparison of RNAi + DHA + H_2O_2 and control + DHA + H_2O_2 treatment histograms shows that RNAi-mediated knockdown of endogenous GLUT10 expression in A10 cells abolished the reduction of ROS in H_2O_2-treated cells preincubated with DHA. (C) A comparison of GLUT10 + insulin + DHA + H_2O_2 and GLUT10 + DHA+ H_2O_2 treatment histograms shows that insulin stimulation, which induces GLUT10 translocation to mitochondria, further reduced ROS production in adipocytes incubated with DHA under oxidative stress conditions. (**D**) Total ascorbate accumulation in mitochondria was determined by HPLC (as described in Materials and Methods) in empty vector (open box, control)- or GLUT10/Myc-His (filled box, GLUT10)-transfected A10 cells cultured with 1 mM DHA (DHA) or DHA and H_2O_2 (DHA + H_2O_2). Mitochondrial ascorbate levels were increased in cells incubated with DHA and were further increased in cells incubated with DHA under oxidative stress conditions. Ascorbate levels in mitochondria of GLUT10-expressing A10 cells were significantly increased compared with those in control cell mitochondria under DHA and oxidative stress conditions (DHA + H_2O_2). (**E**) RNAi-mediated knockdown of endogenous GLUT10 expression. Endogenous GLUT10 mRNA expression levels in A10 cells were determined by real-time RT–PCR; the relative expression levels are shown. CN, A10 cells transfected with Negative Universal Control oligonucleotides; glut10 RNAi, A10 cells transfected with glut10RNAi.

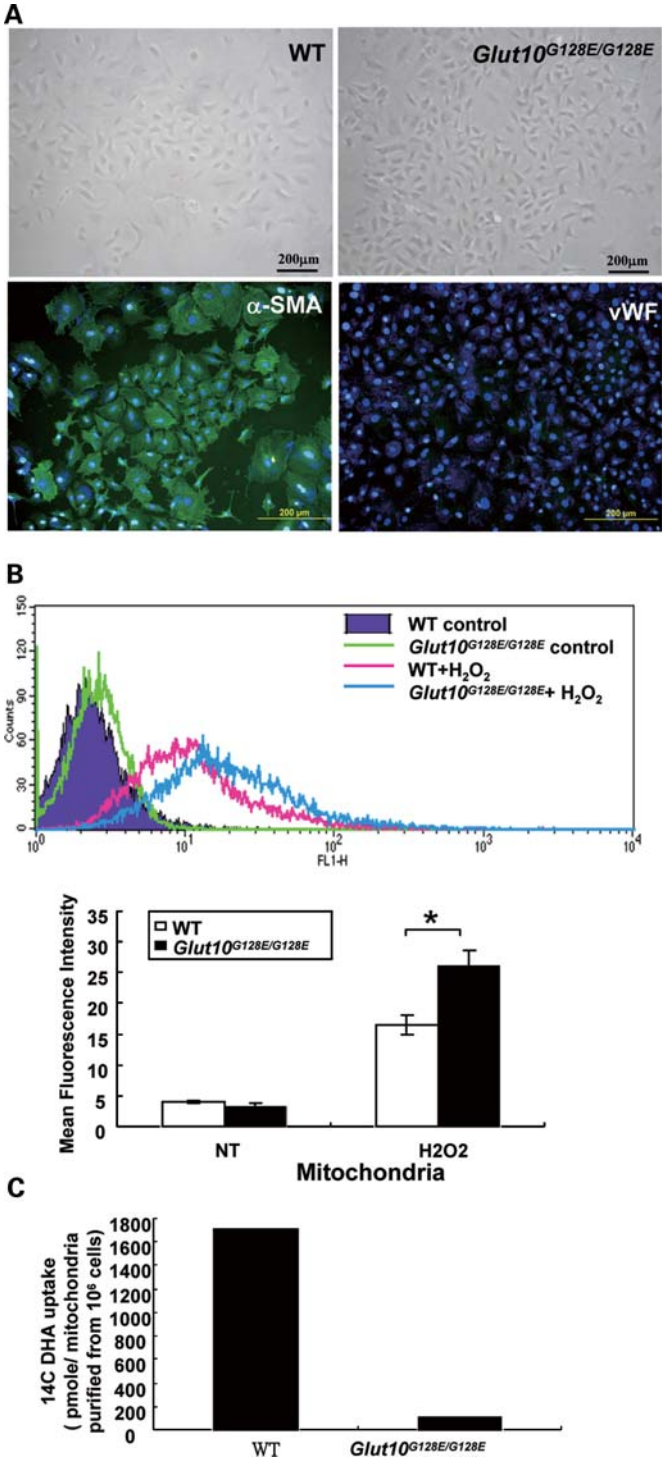

Figure 6. Intracellular ROS levels and DHA-uptake ability in aortic smooth muscle cells from *Glut10*$^{G128E/G128E}$ mice and wild-type littermates. (**A**) Aortic smooth muscle cells (ASMCs) from *Glut10*$^{G128E/G128E}$ mice and wild-type littermates exhibited comparable, normal morphology, and were positive for the vascular smooth muscle cell marker α-smooth muscle actin (α-SMA), and negative for the endothelial marker von Willebrand factor (vWF) in both genotypes. (**B**) Intracellular ROS production in cells under normal or stressed conditions was detected by H_2DCFDA-staining and analyzed by flow cytometry. The results of overlay histograms from one representative experiment (of three independent experiments) performed using samples prepared from different mice are presented. Quantitative data are shown below the histograms. ROS levels in ASMCs were higher in *Glut10*$^{G128E/G128E}$ mice than in wild-type littermates under oxidative stress conditions. (**C**) DHA-uptake ability, assayed by incubating purified mitochondria with 0.4 mM ^{14}C-labeled DHA, was lower in mitochondria of ASMCs from *Glut10*$^{G128E/G128E}$ mice than in those from wild-type littermates. (Pooled smooth muscle cells from three individual mice for each genotypes.)

of 10 months (12). Aortic smooth muscle cells were isolated from *Glut10*$^{G128E/G128E}$ mice and their wild-type littermates. The identity of these cells as smooth muscle was confirmed by positive staining for the vascular smooth muscle marker α-smooth muscle actin (α-SMA), and endothelial cell contamination was examined by staining for the endothelial cell marker von Willebrand factor (vWF) (Fig. 6A). The morphology of aortic smooth muscle cells cultured from *Glut10*$^{G128E/G128E}$ mice was normal (Fig. 6A). However, intracellular ROS levels were higher in aortic smooth muscle cells from *Glut10*$^{G128E/G128E}$ mice than in those from wild-type littermates under oxidative stress conditions (Fig. 6B). The DHA-uptake ability of mitochondria purified from aortic smooth muscle cells of *Glut10*$^{G128E/G128E}$ mice was reduced compared with that in the wild-type (Fig. 6C). These results indicate that the functionally deficient GLUT10 in *Glut10*$^{G128E/G128E}$ mice impaired DHA entry into mitochondria, leading to increased intracellular ROS levels and, subsequently, abnormal elastogenesis.

DISCUSSION

To investigate the function of GLUT10 and identify possible mechanisms by which GLUT10 loss-of-function mutations lead to ATS, we first identified cell-type-specific expression and subcellular localization of GLUT10. GLUT10 mRNA is highly expressed in aortic smooth muscle cells and in white adipose tissues in humans and mice. GLUT10 primarily localizes to mitochondria in smooth muscle cells; in adipocytes, GLUT10 localizes to the Golgi apparatus under basal conditions and translocates to mitochondria upon insulin stimulation. These data indicate that GLUT10 subcellular localization, which is an important indicator of potential function, differs according to both environmental conditions and specific cell types.

To assess the DHA transport function of GLUT10 in mitochondria, we determined DHA entry into mitochondria in GLUT10/EGFP-expressing A10 cells and insulin-stimulated, GLUT10/EGFP-expressing 3T3-L1 cells. Because under normal conditions DHA is reduced to ascorbate by cytosolic-reducing mechanisms after entering cells, we used a higher-than-physiological concentration of DHA in these uptake experiments. Compared with EGFP-expressing control cells, the amount of DHA entering mitochondria was higher in GLUT10-expressing A10 cells, particularly in the presence of high concentrations of DHA (Fig. 4A). Moreover, insulin stimulation significantly increased DHA entry into the mitochondria of 3L3-L1 cells, reflecting insulin-induced GLUT10 mitochondrial localization (Fig. 4F). Total ascorbate levels also increased in the mitochondria of H_2O_2-treated A10 cells (Fig. 5D), indicating that mitochondrial GLUT10 might play an important role in cells exposed to oxidative stress, a condition in which cytosolic DHA concentrations might

increase. The DHA-uptake ability of GLUT10 in mitochondria was also confirmed using a purified mitochondria system (Fig. 4C, D and E), which was capable of demonstrating a concentration- and time-dependent increase in mitochondrial DHA uptake in A10 cells exogenously expressing GLUT10. To our knowledge, this is the first functional DHA transporter demonstrated in the mitochondria of physiological relevant cells.

Importantly, our demonstration that mitochondrial GLUT10 functions mainly as a DHA transporter in smooth muscle cells and adipocytes provides a possible explanation for long-standing questions about the mechanism(s) of vitamin C entry into mitochondria. High accumulations of vitamin C in mitochondria have been detected in rat liver and brain (20,21), and vitamin C has been suggested to be the preferential reducing agent in yeast mitochondria (22). However, the precise mechanism(s) responsible for mediating vitamin C transport into mitochondria have remained poorly understood. Mammalian mitochondria cannot transport ascorbate (18,19), but plant and mammalian mitochondria have been suggested to transport vitamin C in its oxidized form, DHA, through the glucose transporter (19,23). GLUT1, in particular, has been proposed to play such a role in mammalian cells, based on mitochondrial localization in 293T and NIH3T3 cells (19). However, the DHA transport function of GLUT1 in mitochondria has not yet been demonstrated. It has also been shown that GLUT1 is mainly expressed on the plasma membrane of erythrocytes and endothelial cells of the blood–brain barrier, as well as in transformed cells; in each case, its expression correlates with increased cellular uptake of glucose (2). GLUT1 was recently shown to be a major transporter for DHA uptake on the plasma membrane of erythrocytes, especially in non-vitamin-C-producing mammals (24).

To examine the possibility that another glucose transporter might also locate to mitochondria in aortic smooth muscle cells and function as a DHA transporter, we examined the subcellular localization of three GLUTs in aortic smooth muscle cells. GLUT1 has been shown to be localized to the mitochondria in 293T cells and NIH3T3 cells. GLUT6 and GLUT8 also belong to glucose transporter class III, and have been shown to localize to intracellular compartments in several cell types (25,26). We generated expression constructs for the corresponding GLUT/EGFP fusion proteins in which EGFP was fused to the C-terminus of GLUT1, GLUT 6 or GLUT 8 (Supplementary Material, Fig. S5A), and examined their mitochondrial localization in A10 cells by co-localization with a mitochondria tracker. None of the GLUT/EGFP fusion proteins showed a mitochondrial localization pattern in A10 cells (Supplementary Material, Fig. S5B), providing additional support for a critical role for GLUT10 in DHA transport into mitochondria in aortic smooth muscle cells.

We observed that in addition to enhancing DHA entry into mitochondria, DHA uptake was significantly increased in GLUT10/EGFP-expressing A10 cells incubated with DHA (Fig. 4B). Mitochondrial ascorbate levels were also significantly increased in A10 cells exposed to oxidative stress in the presence of DHA, and were further increased in A10 cells expressing GLUT10 under the same conditions (Fig. 5D). These results indicate that mitochondrial GLUT10

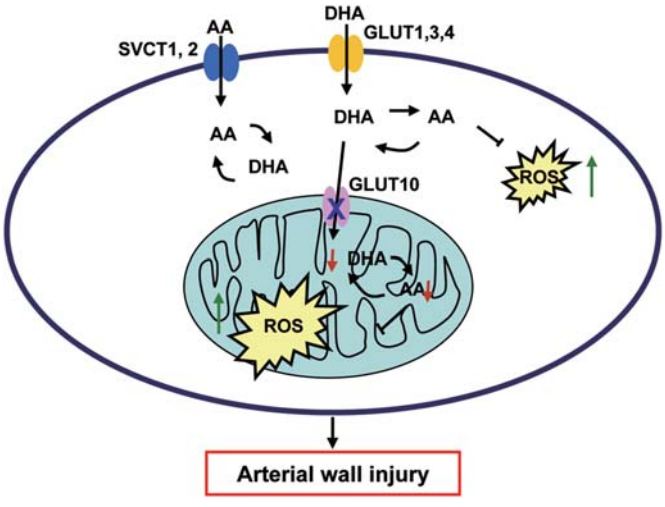

Figure 7. Model depicting how loss-of-function GLUT10 mutations may disturb vitamin C homeostasis and cellular antioxidants in aortic smooth muscle cells. Vitamin C is transported into the cell in its reduced (ascorbate, AA) and oxidized (DHA) forms by active sodium vitamin C transporter 1, 2 (SVC1, 2) and facilitative glucose transporters 1, 3, 4 (GLUT 1, 3, 4), respectively. Under normal conditions, most DHA in the cytosol is reduced to ascorbate. However, under oxidative stress conditions, DHA might accumulate in cytosol and then be transported into mitochondria by mitochondrial GLUT10, where it is regenerated into ascorbate. The ascorbate quenches ROS and protects cells from oxidative stress. Loss-of-function GLUT10 mutations (indicated by X on GLUT10) impair DHA transport into mitochondria, leading to reduce DHA uptake (indicated by red down arrows) and increased cellular and mitochondrial ROS levels (indicated by green up arrows) under oxidative stress conditions. The decrease of DHA transport into mitochondria and increase in ROS have direct effects on the arterial wall and cell signaling (see Discussion), leading to fragmentation and disorganization of elastic fibers, and remodeling of smooth muscle cells in aortic tissue, ultimately cascading into cardiovascular injury in ATS.

might play an important role under oxidative stress conditions, specifically, by enhancing the entry of cytosolic DHA into the mitochondria, and thereby protect cells against oxidative stress. As illustrated in Figure 7, vitamin C is transported into the cell in both reduced (ascorbate) and oxidized (DHA) forms by active sodium vitamin C transporter 1 or 2 (SVCT1, 2), facilitative GLUT1 and GLUT3 and, to a lesser extent, by GLUT4. Under normal conditions, most DHA in the cytosol is reduced to ascorbate. However, under oxidative stress conditions, DHA might accumulate in cytosol and then be transported into mitochondria by mitochondrial GLUT10, where it is regenerated into ascorbate by several mechanisms (27–29). The glutathione (GSH)-dependent reduction of DHA seems to be the most prominent mechanism (18), consistent with the high concentrations of GSH (up to 5–10 mM) observed in mitochondria (30,31). Reduced ascorbate protects mitochondria from oxidative stress (19). The entry of DHA into mitochondria might play an important role in maintaining cellular redox homeostasis under stress condition. Our finding that GLUT10 mediates DHA transport into mitochondria provides a possible contributing mechanism to vitamin C in mitochondria and redox metabolism under oxidative stress in cells.

The loss-of-function GLUT10 mutant disrupted DHA entry into mitochondria, which increased ROS levels in cells, especially under stress conditions. The disturbance of redox status might lead to ATS (Fig. 7). The increase of harmful

ROS has been shown relevant for the onset and progression of degenerative diseases such as cardiovascular disease (32). Increasing evidence indicates that ROS play a major role in mediating distinct physiological and pathophysiological effects in each of the vascular cell types involved in the initiation and progression of cardiovascular dysfunction. In vascular smooth muscle cells, ROS promote apoptosis, migration and proliferation, and also modulate expression of inflammatory genes, degradation of matrix components and cellular reorganization—all prominent events in pathogenic vascular remodeling and aortic aneurysms (33–35). These phenotypes were observed in ATS patients, thus suggesting that GLUT10 is involved in DHA entering mitochondria and redox homeostasis under oxidative stress and contributed to vascular pathogenesis and aortic aneurysms. Further studies in the GLUT10-mutant mouse model will be performed to determine the detailed molecular mechanisms underlying the relationship between deficiency of mitochondrial DHA transport and ATS.

Our demonstration that GLUT10 is highly expressed and translocates to mitochondria in response to insulin stimulation, thereby mediating DHA transport into mitochondria and reducing ROS production under oxidative stress conditions in adipocytes, clarifies the link between GLUT10 and type 2 diabetes. It has been suggested that high glucose levels in type 2 diabetic patients increase ROS production (36), and that increased ROS production in adipocytes is the trigger for insulin resistance in type 2 diabetes patients (37,38). Therefore, we suggest that the insulin-stimulated translocation of GLUT10 to mitochondria in adipose tissue is important for maintaining redox homeostasis, especially under hyperglycemic conditions. We propose that single-nucleotide polymorphisms of GLUT10 that influence GLUT10 expression level, mitochondrial targeting or DHA transport function might affect the progression of insulin resistance in type 2 diabetic patients.

In summary, we have demonstrated the mitochondrial localization of GLUT10 and shown that GLUT10 functions as a DHA transporter in physiologically relevant cells. We have also provided a mechanism to account for the involvement of GLUT10 in vitamin C and redox homeostasis under oxidative stress condition. Importantly, our findings provide a molecular framework for understanding the pathogenesis of ATS, and provide new insights into the relationship between GLUT10 and type 2 diabetes.

MATERIALS AND METHODS

RNA isolation and quantitative real-time RT–PCR analysis

Total RNA from various tissues of 20-week-old C3HeB/FeJ wild-type mice was isolated using the TRIzol reagent (Invitrogen). Total RNA was further purified with QIAGEN RNeasy Mini Kit, treated with DNase (DNase I, 30 U/μg total RNA; QIAGEN), and reverse-transcribed using the SuperScript III First-Strand Synthesis System (Invitrogen). Tissue levels of GLUT10 mRNA and the inhibition efficiency of GLUT10-specific RNAi were determined by quantitative detection of GLUT10 mRNA levels by real-time RT–PCR using SYBR Green PCR Master Mix and an ABI Prism 7900HT Sequence Detection System (Applied Biosystems). The primers used for RT–PCR are described in Supplementary Material. GLUT10 mRNA tissue expression and GLUT10 RNAi inhibition data normalized to β-actin and GAPDH, respectively, are presented as relative expression levels. Three individual animals were used for the determination of GLUT10 mRNA tissue expression, and three independent experiments were used to analyze RNAi-mediated GLUT10 knockdown.

Detection of GLUT10 mRNA expression in mouse aorta by *in situ* hybridization

An *Slc2A10* cDNA fragment (corresponding to nucleotides 567–1413 of GeneBank accession number NM_130451) was amplified from mouse liver cDNA and subcloned into the pBluescript SK(−) vector. The primer pairs used for the amplification are described in Supplementary Material. The plasmids were linearized, and the sense and antisense probes were *in vitro*-transcribed using an AmpliScribe™ T7-*Flash*™ Transcription Kit (EPICENTRE Biotechnologies) and labeled with digoxigenin-11-UTP (Roche Diagnostics). GLUT10 mRNA in sections prepared from flash-frozen mouse aortas was analyzed by *in situ* hybridization according to a previously described protocol (39) with minor modifications (described in Supplementary Material). The tissues were visualized using standard light microscopy.

Immunohistochemistry

For immunohistochemical staining of aortic desmin, mouse aortas were fixed in 4% paraformaldehyde (PFA) and sectioned. The sections were treated with 0.3% H_2O_2 and incubated with anti-desmin monoclonal antibody (1:500; Sigma) overnight at 4°C. After incubation, the slides were washed and further incubated with anti-mouse biotinylated secondary antibody (1:500; Vector Laboratories) for 1 h. The washed sections were then incubated with ABC complex following the manufacturer's protocol (Vector Laboratories). The tissues were air-dried, mounted with mounting medium and visualized by standard light microscopy.

Cell culture and transfection

A10 rat aortic smooth muscle cells and 3T3-L1 murine preadipocytes were grown in Dulbecco's modified Eagle medium (DMEM; Gibco) containing 25 mM glucose supplemented with 10% fetal bovine serum (FBS; Biological Industries), 10% calf serum (Hyclone), 1% penicillin/streptomycin (Gibco) and 2 mM L-glutamine (Gibco). For insulin stimulation, the cells were starved in FBS-free, low-glucose (5 mM) DMEM for 24 h, and then stimulated with the indicated concentration of insulin for 24 h. All transfections of A10 and 3T3-L1 cells were carried out using Effectene (QIAGEN, Hilden, Germany), as described by the manufacturer. The overall transfection rate in both cell types is >70%. A rat GLUT10-specific RNAi (Rat SLC2A10 XM_345741; Invitrogen) and control RNAi (Negative Universal Control; Invitrogen) were used for GLUT10 knockdown experiments in A10 cells.

Plasmid construction

The full-length mouse *Slc2A10* cDNA was amplified and inserted into the pEGFP-N1 expression vector (Clontech) or pcDNA4/Myc-His (Invitrogen) to express GLUT10/EGFP or GLUT10/Myc-His fusion proteins, respectively. Full-length cDNAs encoding mouse GLUT10, GLUT 6 and GLUT8 were amplified from mouse liver cDNA and inserted into the pEGFP-N1 expression vector (Clontech) to yield the respective GLUT1-EGFP, GLUT6-EGFP and GLUT8-EGFP fusion constructs. The primer pairs used for the construction of the expression vector are indicated in Supplementary Material. The pEGFP-N1 expression vector was used as an EGFP-only control. The pcDNA4/Myc-His vector was used as a transfection control in ROS assays.

Co-localization of GLUT10 with intracellular compartments

Cells were seeded in glass culture dishes (Warner Instruments), washed and incubated at 37°C for 40 min with prewarmed staining buffer containing 200 nM endoplasmic reticulum (ER) marker (ER-Tracker™ Red dye; Molecular Probes), 100 nM mitochondria marker (M7510; Molecular Probes) or Golgi marker (BODIPY Dye; Molecular Probes). Cells were then washed and fresh medium was added. Live-cell images were collected using an UltraView fluorescence detection system (PerkinElmer). For immunofluorescence staining, the cells were grown on chamber slides and fixed with 3.6% PFA in PBS, then stained with monoclonal mouse anti-His antibody (1:200; Abcam). The signals were then monitored by fluorescence detection of FITC-conjugated secondary antibodies. Images were observed and collected using a Radiance-2100 laser-scanning confocal microscope (Bio-Rad).

Establishment of stably transfected 3T3-L1 cell lines, differentiation of preadipocytes and insulin stimulation

Vectors expressing GLUT10/EGFP or EGFP were transfected into 3T3-L1 cells, and stably transformed cell lines were selected by culturing in the presence of appropriate antibiotics. 3T3-L1 preadipocytes were cultured and induced to differentiate as described previously (40) with minor modifications (described in Supplementary Material). Differentiated 3T3-L1 adipocytes were stained with Oil-Red-O to demonstrate the presence of triglyceride droplets (40). GLUT10 translocation was induced by treating differentiated 3T3-L1 cells with 10 μg/ml insulin for 24 h before the translocation assay.

Subcellular fractionation into mitochondrial, Golgi and ER fractions

3T3-L1 adipocytes were fractionated following a previously described protocol (41). The mitochondrial fraction of A10 cells was isolated using a mitochondria isolation kit (Pierce). Proteins were resolved by SDS–PAGE and then transferred to polyvinylidene difluoride membranes. After blocking, membranes were incubated with primary antibodies against EGFP (1:1000; Millipore) to detect GLUT10/EGFP, and with antibodies against the Golgi and mitochondrial markers TGN38 C-15 (1:1000; Santa Cruz) and Hsp60 (1:1000; Chemicon). After washing, membranes were incubated with horseradish peroxidase-conjugated secondary antibodies, and proteins were visualized using an enhanced chemiluminescence detection system (Amersham Biosciences).

^{14}C-Labeled DHA and ^{14}C-labeled D-glucose uptake into cells or mitochondria

^{14}C-labeled DHA was produced by incubating 10 mM ^{14}C-labeled ascorbic acid (diluted from 250 μCi stock, 7 mCi/m mol; PerkinElmer) with 5 μl ascorbic acid oxidase (100 μ/ml stock; Sigma) in a 50 μl reaction at 37°C for 1 min. Using HPLC (described below) to monitor the efficiency of ascorbic acid oxidation (measured as the decrease in ascorbic acid), we confirmed 100% conversion of ascorbic acid to DHA. Cells were incubated in incubation medium (5 mM glucose DMEM without FBS) with the indicated concentration of ^{14}C-labeled DHA for 30 min. Cells were washed and lysed, and ^{14}C counts in total cell lysates were determined by scintillation spectroscopy (Beckman-Coulter). ^{14}C entry into mitochondria was assessed by incubating cells for 30 min in incubation medium containing the indicated concentration of ^{14}C-labeled DHA or ^{14}C-labeled glucose (50 μCi/m mol; PerkinElmer). The cells were then washed and used for preparing cytosol extracts and purified mitochondria. For the uptake of DHA into purified mitochondria, mitochondria from control A10 cells (transfected with empty vector) or A10 cells expressing EGFP or GLUT10/EGFP were purified using a mitochondria isolation kit (Pierce). Purified mitochondria were incubated for the indicated time (routinely 30 min) in incubation buffer (15 mM HEPES, 135 mM NaCl, 5 mM KCl, 1.8 mM $CaCl_2$, 0.8 mM $MgCl_2$, pH 7.4) containing the indicated concentration of ^{14}C-labeled DHA. Mitochondria were then washed and lysed, and ^{14}C counts were determined. ^{14}C entry into cells or mitochondria was expressed as moles DHA or glucose in 30 min per cell amount calculated from counts by reference to a standard curve prepared using serial dilutions of a known amount of ^{14}C-labeled DHA or D-glucose. For D-glucose competition assays, purified mitochondria were preincubated with the indicated concentration of D-glucose for 30 min before the addition of ^{14}C-labeled DHA.

Measurement of ascorbic acid accumulation by HPLC

Samples for HPLC determination of total intracellular ascorbic acid levels were prepared by incubating cells in incubation medium with the indicated concentration of DHA for 30 min at 37°C. After incubation, the cells were washed with Hank's balanced salt solution (HBSS) and lysed in 200 μl ice-cold 60% HPLC-grade methanol (Merck). Total cell lysates were centrifuged at 12 000 rpm at 4°C (F45-24-11 rotor, Centrifuge 5415R; Eppendorf), and supernatants were collected and filtered through 0.45 μm nylon membrane filters (Millipore). Samples for the determination of ascorbic acid levels in mitochondrial fractions were prepared by purifying mitochondria from cells, using a mitochondria isolation kit (Pierce) and processing as described above for whole cells. Samples were separated using a modified C18 column

(SunFire^{TM} C18 3.5 μm, 3.0 × 150 mm column, Waters) and detected with a UV detector (Waters 2487) at a wavelength of 254 nm. The column was equilibrated at 25°C with equilibration buffer consisting of 50 μM sodium phosphate (Sigma), 50 μM sodium acetate (Sigma), 189 μM dodecyltrimethylammonium chloride (Fluka) and 3.66 μM tetraoctylammonium bromide (Fluka) in a 30:70 solution of methanol:ddH_2O (v/v), pH 4.8. Samples (20 μl) were injected and eluted with equilibration buffer at a flow rate of 0.3 ml/min. Under these conditions, the retention time of ascorbic acid is 2.3 min. Ascorbic acid accumulation in cells or mitochondria was presented in picomoles ascorbic acid per 30 min per cell amount by comparing the ascorbic acid chromatographic peak area with a standard curve covering a concentration range of 0.2–1.5 mM ascorbic acid. To determine the specificity of the ascorbic acid peak in the cell lysates, we performed experiments by incubating the cells with different concentrations of DHA, and the increase of ascorbic acid peak area in response to the increasing of extracellularly applied DHA was observed. In addition, incubating the cell lysates with ascorbic acid oxidase, the ascorbic acid peak area decreased in the sample.

Measurement of ROS

ROS levels were determined using the fluorescent probe 2′,7′-dichlorodihydrofluorescein diacetate (DCFH-DA; Sigma). Cells (1×10^5) transfected with a GLUT10/Myc-His expression construct or empty pcDNA4/Myc-His vector were cultured in six-well plates in 5 mM glucose DMEM supplemented with 10% FBS, with or without 1 mM DHA for 1 h. Cells were then washed with HBSS and incubated with DCFH-DA (10 μM) at 37°C for 1 h. After incubation, cells were treated with or without H_2O_2 (0.5 mM) for an additional 1 h, washed with HBSS and resuspended in PBS. The fluorescence intensity of cells was determined by flow cytometry using a FACScan flow cytometer (BD Biosciences). The data were analyzed using FlowJo software and presented quantitatively as the percentage of high-ROS cells relative to the H_2O_2-treated group, where high-ROS cells are defined as those having a fluorescence intensity greater than the mean fluorescence of the H_2O_2-treated group.

Isolation and culture of vascular smooth muscle cells from single mouse aortas

The GLUT10-deficient mouse expressing the missense GLUT10 [G128] mutant was described previously (12). Vascular smooth muscle cells were isolated from single mouse aortas from 6–8-week-old homozygous *Glut10*$^{G128E/G128E}$ mice or their wild-type littermates following previously described methods (42). The purity of aortic smooth muscle cells was confirmed by immunofluorescent staining for the smooth muscle cell- and endothelial cell-specific markers α-SMA (1:200; Sigma) and vWF (1:200; Abcam), respectively. ROS levels were determined under normal and oxidative (1 mM H_2O_2 for 1 h) stress conditions.

Statistical analysis

A two-tailed Student's *t*-test was used to test for differences between treatments. A *P*-value <0.05 was considered statistically significant ($^{*}P$-value <0.05, $^{**}P$-value <0.01, $^{***}P$-value <0.001).

SUPPLEMENTARY MATERIAL

Supplementary Material is available at *HMG* online.

ACKNOWLEDGEMENTS

We thank Dr David Tu, Dr Anil Mukherjee and Dr Gary Zhang for their critical review of the manuscript. We appreciate the technical assistance of Chia-Ying Lin, Chia-Chen Tai and Sheng-De Chen.

Conflict of Interest statement. None declared.

FUNDING

This work was supported by grants from the National Research Program for Genomic Medicine, Taiwan, Republic of China (National Genotyping Core, NSC- 98-3112-B-001-002) and Academia Sinica Genomic Medicine Multicenter Study, Taiwan, Republic of China (5202401129-3).

REFERENCES

1. Joost, H.G. and Thorens, B. (2001) The extended GLUT-family of sugar/polyol transport facilitators: nomenclature, sequence characteristics, and potential function of its novel members (Review). *Mol. Membr. Biol.*, **18**, 247–256.
2. Uldry, M. and Thorens, B. (2004) The SLC2 family of facilitated hexose and polyol transporters. *Pflugers Arch.*, **447**, 480–489.
3. Ghosh, S., Watanabe, R.M., Valle, T.T., Hauser, E.R., Magnuson, V.L., Langefeld, C.D., Ally, D.S., Mohlke, K.L., Silander, K., Kohtamaki, K. *et al.* (2000) The Finland–United States investigation of non-insulin-dependent diabetes mellitus genetics (FUSION) study. I. An autosomal genome scan for genes that predispose to type 2 diabetes. *Am. J. Hum. Genet.*, **67**, 1174–1185.
4. McVie-Wylie, A.J., Lamson, D.R. and Chen, Y.T. (2001) Molecular cloning of a novel member of the GLUT family of transporters, SLC2a10 (GLUT10), localized on chromosome 20q13.1: a candidate gene for NIDDM susceptibility. *Genomics*, **72**, 113–117.
5. Andersen, G., Rose, C.S., Hamid, Y.H., Drivsholm, T., Borch-Johnsen, K., Hansen, T. and Pedersen, O. (2003) Genetic variation of the GLUT10 glucose transporter (SLC2A10) and relationships to type 2 diabetes and intermediary traits. *Diabetes*, **52**, 2445–2448.
6. Bento, J.L., Bowden, D.W., Mychaleckyj, J.C., Hirakawa, S., Rich, S.S., Freedman, B.I. and Segade, F. (2005) Genetic analysis of the GLUT10 glucose transporter (SLC2A10) polymorphisms in Caucasian American type 2 diabetes. *BMC Med. Genet.*, **6**, 42.
7. Lin, W.H., Chuang, L.M., Chen, C.H., Yeh, J.I., Hsieh, P.S., Cheng, C.H. and Chen, Y.T. (2006) Association study of genetic polymorphisms of SLC2A10 gene and type 2 diabetes in the Taiwanese population. *Diabetologia*, **49**, 1214–1221.
8. Mohlke, K.L., Skol, A.D., Scott, L.J., Valle, T.T., Bergman, R.N., Tuomilehto, J., Boehnke, M. and Collins, F.S. (2005) Evaluation of SLC2A10 (GLUT10) as a candidate gene for type 2 diabetes and related traits in Finns. *Mol. Genet. Metab.*, **85**, 323–327.
9. Coucke, P.J., Willaert, A., Wessels, M.W., Callewaert, B., Zoppi, N., De Backer, J., Fox, J.E., Mancini, G.M., Kambouris, M., Gardella, R. *et al.* (2006) Mutations in the facilitative glucose transporter GLUT10

alter angiogenesis and cause arterial tortuosity syndrome. *Nat. Genet.*, **38**, 452–457.
10. Callewaert, B.L., Willaert, A., Kerstjens-Frederikse, W.S., De Backer, J., Devriendt, K., Albrecht, B., Ramos-Arroyo, M.A., Doco-Fenzy, M., Hennekam, R.C., Pyeritz, R.E. *et al.* (2008) Arterial tortuosity syndrome: clinical and molecular findings in 12 newly identified families. *Hum. Mutat.*, **29**, 150–158.
11. Dawson, P.A., Mychaleckyj, J.C., Fossey, S.C., Mihic, S.J., Craddock, A.L. and Bowden, D.W. (2001) Sequence and functional analysis of GLUT10: a glucose transporter in the type 2 diabetes-linked region of chromosome 20q12–13.1. *Mol. Genet. Metab.*, **74**, 186–199.
12. Cheng, C.H., Kikuchi, T., Chen, Y.H., Sabbagha, N.G., Lee, Y.C., Pan, H.J., Chang, C. and Chen, Y.T. (2009) Mutations in the SLC2A10 gene cause arterial abnormalities in mice. *Cardiovasc. Res.*, **81**, 381–388.
13. Al-Hasani, H., Kunamneni, R.K., Dawson, K., Hinck, C.S., Muller-Wieland, D. and Cushman, S.W. (2002) Roles of the N- and C-termini of GLUT4 in endocytosis. *J. Cell Sci.*, **115**, 131–140.
14. Cline, G.W., Jucker, B.M., Trajanoski, Z., Rennings, A.J. and Shulman, G.I. (1998) A novel 13C NMR method to assess intracellular glucose concentration in muscle, *in vivo*. *Am. J. Physiol.*, **274**, E381–E389.
15. Vera, J.C., Rivas, C.I., Fischbarg, J. and Golde, D.W. (1993) Mammalian facilitative hexose transporters mediate the transport of dehydroascorbic acid. *Nature*, **364**, 79–82.
16. Rumsey, S.C., Daruwala, R., Al-Hasani, H., Zarnowski, M.J., Simpson, I.A. and Levine, M. (2000) Dehydroascorbic acid transport by GLUT4 in *Xenopus* oocytes and isolated rat adipocytes. *J. Biol. Chem.*, **275**, 28246–28253.
17. Rumsey, S.C., Kwon, O., Xu, G.W., Burant, C.F., Simpson, I. and Levine, M. (1997) Glucose transporter isoforms GLUT1 and GLUT3 transport dehydroascorbic acid. *J. Biol. Chem.*, **272**, 18982–18989.
18. Li, X., Cobb, C.E., Hill, K.E., Burk, R.F. and May, J.M. (2001) Mitochondrial uptake and recycling of ascorbic acid. *Arch. Biochem. Biophys.*, **387**, 143–153.
19. Sagun, K.C., Carcamo, J.M. and Golde, D.W. (2005) Vitamin C enters mitochondria via facilitative glucose transporter 1 (Glut1) and confers mitochondrial protection against oxidative injury. *FASEB J.*, **19**, 1657–1667.
20. Ingebretsen, O.C. and Normann, P.T. (1982) Transport of ascorbate into guinea pig liver mitochondria. *Biochim. Biophys. Acta*, **684**, 21–26.
21. Fujimoto, Y., Matsui, M. and Fujita, T. (1982) The accumulation of ascorbic acid and iron in rat liver mitochondria after lipid peroxidation. *Jpn J. Pharmacol.*, **32**, 397–399.
22. Monteiro, G., Horta, B.B., Pimenta, D.C., Augusto, O. and Netto, L.E. (2007) Reduction of 1-Cys peroxiredoxins by ascorbate changes the thiol-specific antioxidant paradigm, revealing another function of vitamin C. *Proc. Natl Acad. Sci. USA*, **104**, 4886–4891.
23. Szarka, A., Horemans, N., Banhegyi, G. and Asard, H. (2004) Facilitated glucose and dehydroascorbate transport in plant mitochondria. *Arch. Biochem. Biophys.*, **428**, 73–80.
24. Montel-Hagen, A., Kinet, S., Manel, N., Mongellaz, C., Prohaska, R., Battini, J.L., Delaunay, J., Sitbon, M. and Taylor, N. (2008) Erythrocyte Glut1 triggers dehydroascorbic acid uptake in mammals unable to synthesize vitamin C. *Cell*, **132**, 1039–1048.
25. Lisinski, I., Schurmann, A., Joost, H.G., Cushman, S.W. and Al-Hasani, H. (2001) Targeting of GLUT6 (formerly GLUT9) and GLUT8 in rat adipose cells. *Biochem. J.*, **358**, 517–522.
26. Widmer, M., Uldry, M. and Thorens, B. (2005) GLUT8 subcellular localization and absence of translocation to the plasma membrane in PC12 cells and hippocampal neurons. *Endocrinology*, **146**, 4727–4736.
27. Wells, W.W., Xu, D.P., Yang, Y.F. and Rocque, P.A. (1990) Mammalian thioltransferase (glutaredoxin) and protein disulfide isomerase have dehydroascorbate reductase activity. *J. Biol. Chem.*, **265**, 15361–15364.
28. Xu, D.P. and Wells, W.W. (1996) Alpha-lipoic acid dependent regeneration of ascorbic acid from dehydroascorbic acid in rat liver mitochondria. *J. Bioenerg. Biomembr.*, **28**, 77–85.
29. Rodriguez-Manzaneque, M.T., Tamarit, J., Belli, G., Ros, J. and Herrero, E. (2002) Grx5 is a mitochondrial glutaredoxin required for the activity of iron/sulfur enzymes. *Mol. Biol. Cell*, **13**, 1109–1121.
30. Gaudemer, Y. and Latruffe, N. (1975) Evidence for penetrant and non-penetrant thiol reagents and their use in the location of rat liver mitochondrial D(−)-beta-hydroxybutyrate dehydrogenase. *FEBS Lett.*, **54**, 30–34.
31. Wahllander, A., Soboll, S., Sies, H., Linke, I. and Muller, M. (1979) Hepatic mitochondrial and cytosolic glutathione content and the subcellular distribution of GSH-*S*-transferases. *FEBS Lett.*, **97**, 138–140.
32. Li, Y. and Schellhorn, H.E. (2007) New developments and novel therapeutic perspectives for vitamin C. *J. Nutr.*, **137**, 2171–2184.
33. Griendling, K.K. and FitzGerald, G.A. (2003) Oxidative stress and cardiovascular injury. Part I. Basic mechanisms and *in vivo* monitoring of ROS. *Circulation*, **108**, 1912–1916.
34. Papaharalambus, C.A. and Griendling, K.K. (2007) Basic mechanisms of oxidative stress and reactive oxygen species in cardiovascular injury. *Trends Cardiovasc. Med.*, **17**, 48–54.
35. Satoh, K., Nigro, P., Matoba, T., O'Dell, M.R., Cui, Z., Shi, X., Mohan, A., Yan, C., Abe, J., Illig, K.A. *et al.* (2009) Cyclophilin A enhances vascular oxidative stress and the development of angiotensin II-induced aortic aneurysms. *Nat. Med.*, **15**, 649–656.
36. Nourooz-Zadeh, J., Tajaddini-Sarmadi, J., McCarthy, S., Betteridge, D.J. and Wolff, S.P. (1995) Elevated levels of authentic plasma hydroperoxides in NIDDM. *Diabetes*, **44**, 1054–1058.
37. Houstis, N., Rosen, E.D. and Lander, E.S. (2006) Reactive oxygen species have a causal role in multiple forms of insulin resistance. *Nature*, **440**, 944–948.
38. Matsuzawa-Nagata, N., Takamura, T., Ando, H., Nakamura, S., Kurita, S., Misu, H., Ota, T., Yokoyama, M., Honda, M., Miyamoto, K. *et al.* (2008) Increased oxidative stress precedes the onset of high-fat diet-induced insulin resistance and obesity. *Metabolism*, **57**, 1071–1077.
39. Zaidi, A.U., Enomoto, H., Milbrandt, J. and Roth, K.A. (2000) Dual fluorescent *in situ* hybridization and immunohistochemical detection with tyramide signal amplification. *J. Histochem. Cytochem.*, **48**, 1369–1375.
40. Hirose, T., Kurebayashi, S. and Kasayama, S. (2001) Antiplatelet agent cilostazol potentiates adipocyte differentiation of 3T3-L1 cells. *Atherosclerosis*, **158**, 19–22.
41. Elmendorf, J.S. (2003) Fractionation analysis of the subcellular distribution of GLUT-4 in 3T3-L1 adipocytes. *Methods Mol. Med.*, **83**, 105–111.
42. Ray, J.L., Leach, R., Herbert, J.M. and Benson, M. (2001) Isolation of vascular smooth muscle cells from a single murine aorta. *Methods Cell Sci.*, **23**, 185–188.